Sensorless Speed Measurement of AC Machines using Analytic Wavelet Transform

J. M. Aller

Universidad Simón Bolívar
Dpto. de Conversión y Transporte de Energía
Caracas 1080A - Venezuela

T. G. Habetler, R. G. Harley, R.M. Tallam and S.B. Lee

Georgia Institute of Technology
School of Electrical and Computer Engineering
Atlanta, GA 30332 USA

***Abstract* - A new method for sensorless speed estimation of AC machines, using the analytic wavelet transform of the stator current signal, is proposed for a Direct Torque Control drive. A comparison with results obtained using the short time Fourier transform is included. The proposed method can be implemented in real time on a DSP. The time-frequency resolution obtained and the computation time required by the proposed algorithm are improved in comparison to existing techniques, and the method can be applied over the entire speed range.**

I. INTRODUCTION

Advances in power semiconductor device technology has led to the widespread use of AC drives using advanced control techniques such as field oriented control or direct torque control (DTC). However, in spite of the robustness of variable speed AC drives, the requirement of a shaft mounted speed sensor renders them less attractive.

Estimators, observers and spectral analysis methods [1,2,3,4] are the frequently used techniques for sensorless speed estimation. The performance of speed estimators depends on the accuracy of the machine model and parameter estimator. Observers for speed estimation have a relatively long delay time that can limit speed detection during a transient. The resolution obtained with spectral analysis is restricted by the uncertainty principle represented by the Heisenberg boxes [5], shown in Fig.1. Ridges algorithms [5,6] can solve this problem efficiently.

The short time Fourier transform (STFT) is a practical tool to measure the frequency variations in time. The time-frequency information is contained in plane boxes called atoms, defined by the spread in time and frequency that contain enough energy density to be useful in signal processing. When a classical window is employed (Gaussian, Hanning, Hamming, etc.), the information is spread over a rectangular atom in the time-frequency plane; this atom area is minimum when a Gaussian window is used. In the STFT, the atom rectangle is the same at all time instants for every window, Fig.1.

The instantaneous frequency can be obtained from ridge analysis, thereby increasing the time-frequency resolution of the Heisenberg boxes. This method has been widely applied in sensorless speed estimations of AC machines [2,3,4].

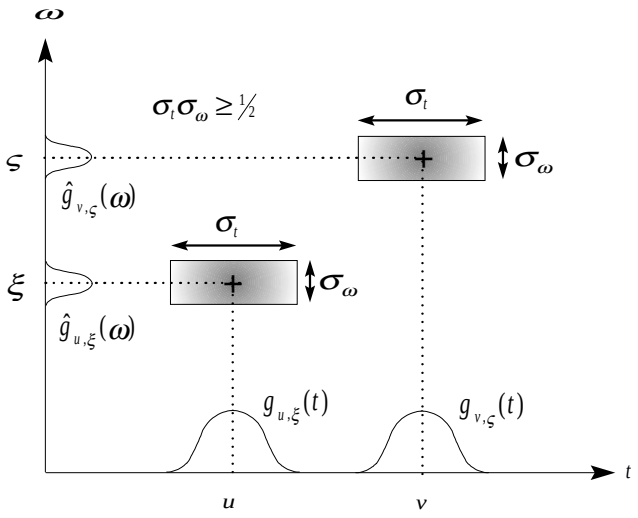

Fig.1. Heisenberg boxes for STFT using the window *g(t)*.

Wavelet analysis is a more general transformation and is also based on internal products of functions. However, in this case the concept of scale replaces the frequency variable of the Fourier Transform. Although the Heisenberg atom area is not smaller than in the STFT with a Gaussian window, the time or frequency resolution can be conveniently changed using different scales, increasing one variable and decreasing the other (equal area atoms). This idea is illustrated in Fig.2.

This additional degree of freedom can improve the angular speed resolution (including the low speed range), in transient or steady state operation. The instantaneous frequency information can be obtained using a few scales appropriately chosen with a base 2 logarithmic distribution, $s^{-1} = \{2, 4, 8, \cdots, 2^m\}$. The

0-7803-6618-8/01/$10.00 (C) 2001 IEEE

ridge algorithm can also be applied in this case to obtain the instantaneous frequency, as with the STFT, to increase the time-frequency resolution [6].

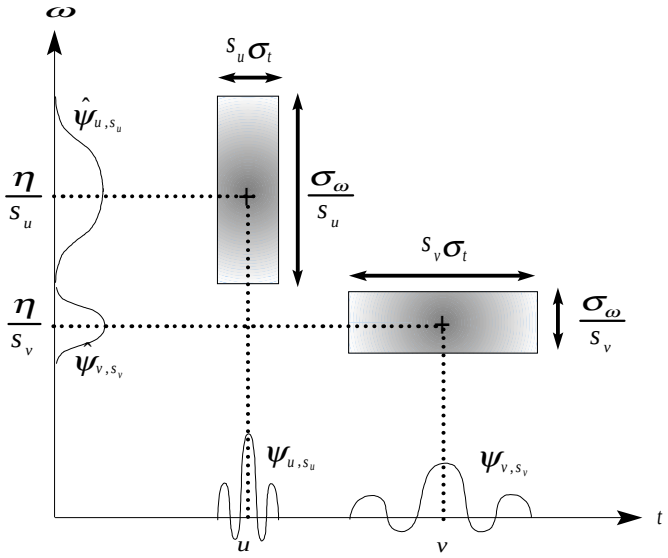

Fig.2. Heisenberg boxes for analytic wavelet transform using two different scales.

In this paper, the stator current of an induction machine with a DTC drive [7,8,9,10], is analyzed using the analytic wavelet transform and the STFT. The results obtained are compared with the angular speed measured with a high-resolution optical encoder.

Wavelet analysis has been applied to reduce torque ripple in DTC drives [11]. Using the same coefficients obtained in this application, the proposed technique can be extended to obtain the angular speed, with just the additional use of the ridges algorithm.

II. Time-Frequency Analysis

A. Short time Fourier transform

The frequency content of the stator current spectrum as a function of time can be analyzed using the STFT, also called windowed Fourier transform (WFT). In the STFT, a Gabor atom, $g_{u,\xi}(t)$, is used to measure the frequency variations in a time signal [2,4,5]. A family of time-frequency Gabor atoms is obtained by modulating the real and symmetric function (window), $g(t)$, by the frequency ξ and translating it by u,

$$g_{u,\xi}(t) = e^{j\xi t} g(t) \tag{1}$$

The STFT of the function $f(t)$ at a particular time, u, and frequency, ξ, is:

$$Sf(u,\xi) = \left\langle f, g_{u,\xi} \right\rangle = \int_{-\infty}^{+\infty} f(t)\ e^{j\xi t} g(t)\ dt \tag{2}$$

The spectrogram of the function $f(t)$ is the energy density of this signal and can be defined as:

$$P_S f(u,\xi) = \left| Sf(u,\xi) \right|^2 \tag{3}$$

The spectrogram can be represented in a three dimensional plot and its ridges represent the instantaneous frequency, $\omega(t)$, [5]:

$$\omega(t) = \tfrac{d}{dt}\phi(t) \geq 0 \tag{4}$$

Where;

$$f(t) = a(t)\cos\phi(t) \quad with \quad a(t) > 0$$

The resolution in time and frequency of the STFT depends on the spread in time and frequency of the selected window (Rectangle, Hamming, Gaussian, Hanning, etc.). This area is minimum (½) when the Gaussian window is used [5].

B. Analytic wavelet transform (AWT)

To analyze the frequency content of the stator current spectrum as a function of time using the wavelet transformation, it is necessary to use an analytic wavelet, $\psi(t)$ [5]. A family of time frequency wavelet atoms is obtained by scaling the wavelet function, ψ, by s and translating it by u,

$$\psi_{u,s}(t) = \tfrac{1}{\sqrt{s}}\psi\left(\tfrac{t-u}{s}\right) \tag{5}$$

The wavelet transform of $f(t)$ at a particular time, u, and scale, s, is,

$$Wf(u,s) = \left\langle f, \psi_{u,s} \right\rangle = \int_{-\infty}^{+\infty} f(t)\, \tfrac{1}{\sqrt{s}}\psi^*\left(\tfrac{t-u}{s}\right) dt \tag{6}$$

The Fourier-Parseval formula can be used to calculate the wavelet transform using the frequency information,

$$Wf(u,s) = \int_{-\infty}^{+\infty} f(t)\psi^*_{u,s}(t)\ dt = \tfrac{1}{2\pi}\int_{-\infty}^{+\infty} \hat{f}(\omega)\ \hat{\psi}^*_{u,s}(\omega)\ d\omega \tag{7}$$

An analytic wavelet can be constructed by modulating the frequency ($e^{j\eta t}$) of a real and symmetric window $g(t)$. A Gabor wavelet $\psi(t) = g(t)e^{j\eta t}$ is obtained from a Gaussian window,

$$g(t) = (\sigma^2\pi)^{-\frac{1}{4}} \exp(\frac{-t^2}{2\sigma^2}) \quad (8)$$

If $\sigma^2\eta^2 >> 1$, then $\hat{g}(\omega) \approx 0$ for $|\omega| > \eta$, and the wavelet function can be considered approximately analytic. The Fourier transform of the Gaussian window (8) is,

$$\hat{g}(\omega) = (4\pi\sigma^2)^{\frac{1}{4}} \exp(-\frac{\sigma^2\omega^2}{2}) \quad (9)$$

The Fourier transform of the Gabor wavelet is,

$$\hat{\psi}(\omega) = \hat{g}(\omega - \eta) \quad (10)$$

The Fourier transform of $\psi_{u,s}$ is a dilation of $\hat{\psi}(\omega)$ by $1/s$, and can be obtained as,

$$\hat{\psi}_{u,s}(\omega) = \sqrt{s}\hat{\psi}(s\omega)\exp(-j\omega\, u) \quad (11)$$

The inverse Fourier transform of the frequency function obtained by multiplying $\hat{f}(\omega)$ with $\sqrt{s}\hat{\psi}(s\omega)$, is directly the AWT, $Wf(u,s)$. Equations (7) and (11) give a simple and fast method to obtain the AWT using the classic FFT algorithm. If an analytic wavelet function is chosen, its Fourier transform is known; hence, computational complexity can be reduced by using the FFT to obtain the Fourier transform of $f(t)$ and the inverse Fourier transform for each scale, s, under analysis. The number of required scales depends on the frequency spectrum being analyzed.

An analytic wavelet transform defines a local time-frequency energy density,

$$P_W\ f\ (u\ ,\ s\ )\ =\ \left|Wf\ \ (u\ ,\ s\ )\right|^2 \quad (13)$$

This energy density is called a scalogram and can be represented on a three-dimensional plot. The instantaneous frequency $\xi(t)$ can be obtained directly from the ridge algorithm defined over the scalogram [6]. The instantaneous frequency $\xi(t)$ is related to the ridges of the normalized scalogram, $s^{-1}P_W f(u,s)$, as,

$$\xi(u) = \eta / s(u) \quad (14)$$

The scalogram defined in (13) is linear in the time axis, but logarithmic (base 2) in the scale axis. To obtain a linear frequency spectrogram, similar to (3), logarithmic interpolation and application of (14) are required.

C. Ridges algorithm

The instantaneous frequency defined in (4) can be estimated by ridges detection in the spectrogram. The spectrogram can be obtained using any time-frequency transform such as: STFT, AWT or Wigner-Ville. However, the signal, $f(t)$, can contain several spectral lines. In this case some additional considerations are necessaries for frequency discrimination. Suppose that the signal is composed of several frequency components,

$$f(t) = \sum a_k(t)\cos\phi_k(t) \quad (15)$$

where $a_k(t)$ and $\phi_k'(t)$ have small variations over the intervals of size s and $s\phi_k'(t) \geq \Delta\omega$. Each instantaneous component can be discriminated by the STFT if the frequency difference is larger than the bandwidth of the Fourier transform of the Gaussian window, $\hat{g}(s\omega)$ [5,6],

$$\left|\phi_i'(u) - \phi_j'(u)\right| \geq \frac{\Delta\omega}{s} \quad (16)$$

If AWT is applied, instantaneous frequencies can be discriminated when the following bandwidth relation is satisfied [5],

$$\frac{\left|\phi_i'(u) - \phi_j'(u)\right|}{\phi_i'(u)} \geq \frac{\Delta\omega}{\eta} \ \ and \ \frac{\left|\phi_i'(u) - \phi_j'(u)\right|}{\phi_j'(u)} \geq \frac{\Delta\omega}{\eta} \quad (17)$$

Relations (16) and (17) are useful tools for selecting scales and bandwidth for the wavelet and Gabor functions.

The ridge algorithm determines instantaneous frequencies from local maxima on the spectrogram $P_S f(u,\xi)$. For this reason, the scalogram must be linearized in the wavelet analysis.

III. Experimental Results

A DTC system was developed using a commercial DSP platform (based on TMS320C44 floating point DSP – max. 60 MFLOPS) that includes four 16-bit A/D converters (200 kHz per channel) and 32 bits of digital I/O. The DSP was programmed to obtain line-to-line voltages, and line currents of an inverter fed 5.0 HP, 208 V, 1760 rpm, 60 Hz, squirrel cage motor. Inverter transistors are activated by six digital outputs generated by the DSP. The sampling frequency was chosen to be 10 kHz. Data acquisition and generation of IGBT gate

drives for the DTC scheme are performed during the 100 μs window. The electromagnetic torque and the stator flux are defined as references. These variables are estimated using the instantaneous voltages and currents measured at the machine terminals. The stator line-to-line voltages are estimated by measuring the DC bus voltage and the inverter switching state at any instant. The stator flux vector is obtained by integrating the terminal voltage,

$$\vec{\lambda}_s = \int_o^t \vec{e}_s \; dt = \int_o^t \left(\vec{v}_s - R_s \vec{i}_s\right) dt \qquad (18)$$

Where:

$$\vec{v}_s \equiv \frac{\sqrt{2}}{3} e^{-j\frac{\pi}{6}} \left(v_{ab} + v_{bc}\, e^{j\frac{2\pi}{3}} + v_{ca}\, e^{j\frac{4\pi}{3}}\right)$$

$$\vec{i}_s \equiv \sqrt{\frac{2}{3}} \left(i_a + i_b\, e^{j\frac{2\pi}{3}} + i_c\, e^{j\frac{4\pi}{3}}\right)$$

The torque is estimated directly as,

$$T_e = \vec{\lambda}_s \times \vec{i}_s \qquad (19)$$

Errors between reference and estimated values of torque and flux are used to switch the inverter devices according to the classical DTC scheme [7,8,9,10].

The squirrel cage motor is started without load, using 3.0 Nm as the reference torque and 0.6 Wb as the flux reference. After the acceleration process, the torque is not maintained at its reference value; the DTC algorithm can only adjust the stator flux when the final speed is reached. Fig.3 shows the electric torque during the no-load start up of the induction motor at constant torque and flux ($0.0 \le t \le 1.0\,s$). Fig.4 shows the space vector diagram of the stator flux under the same condition.

An optical incremental encoder with 1024 ppt is coupled to the motor shaft to perform a direct measure of the angular speed. The DTC algorithm reads the incremental count each 10 ms and calculates the speed. Fig.5 shows that the angular speed obtained by the encoder. Observe that the speed increase is not linear, even though the average torque during this time is constant. This is due to the non-linearity of the mechanical load in the low speed range (static and dynamic friction).

Fig.6 shows the current in one phase during the start up. The stator current has some harmonic components related to the inverter operation (variable frequency commutation), and others given by the slot harmonics.

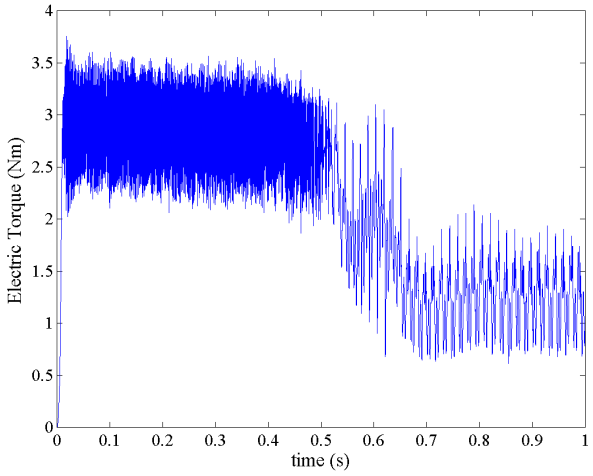

Fig.3. Instantaneous electromagnetic torque during start up with a DTC drive (constant torque and flux references).

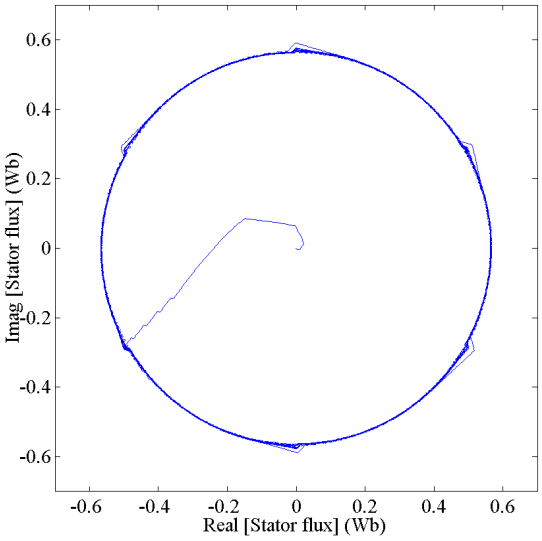

Fig.4. Space vector of the stator flux during start up with a DTC drive (constant torque and flux references).

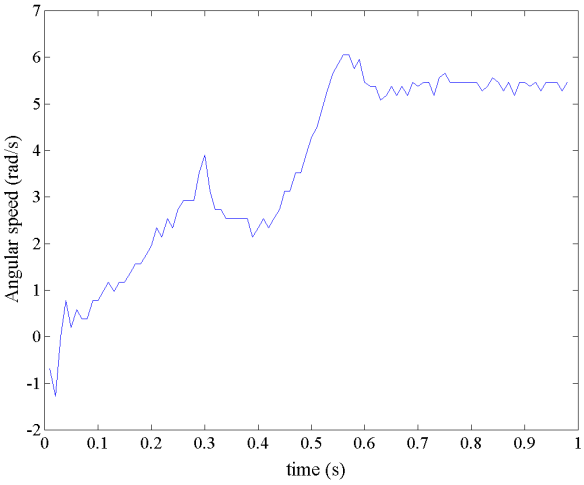

Fig.5. Angular speed of the induction machine during start up measured with an optical encoder.

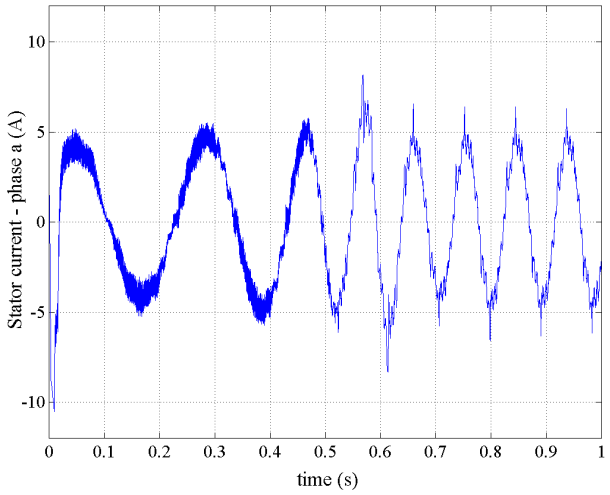

Fig.6. Stator current of the induction machine during a DTC start up with constant torque and flux references.

A digital, second order Butterworth band pass filter (50 Hz – 500 Hz) is used to preprocess the stator current signal. In this way, some interference frequencies coming from the inverter as well as the fundamental component are eliminated. The filtered signal is shown in Fig.7.

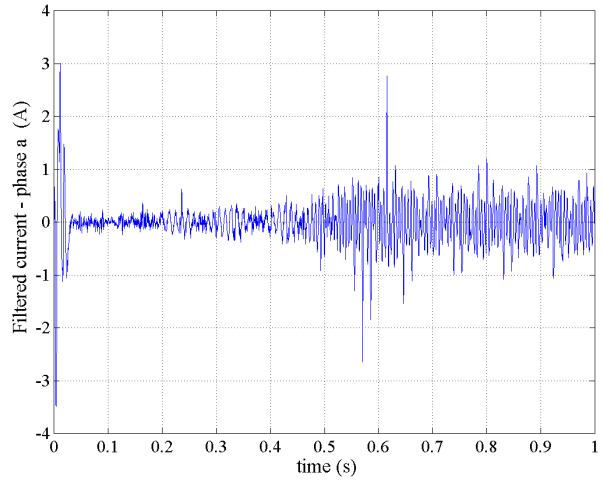

Fig.7. Stator current processed by the second order butterworth band pass filter.

The filtered signal in Fig.7 has information about the slot harmonics and hence, angular speed. The spectrogram $P_S f(u,\xi)$ shown in Fig. 8, is obtained using a Gaussian window with 50 points. Fig. 9 shows the instantaneous frequencies after the use of the ridges algorithm and contains areas of no information, or breaks in the curves. This is due to interference from the inverter produced harmonics. Fig. 10 contains the details of the spectrogram at the time instant t=0.5 s, to illustrate the ridges detection in Fig. 9. It is clear that the use of the ridges algorithm improves the frequency resolution from Fig. 8 to Fig. 9.

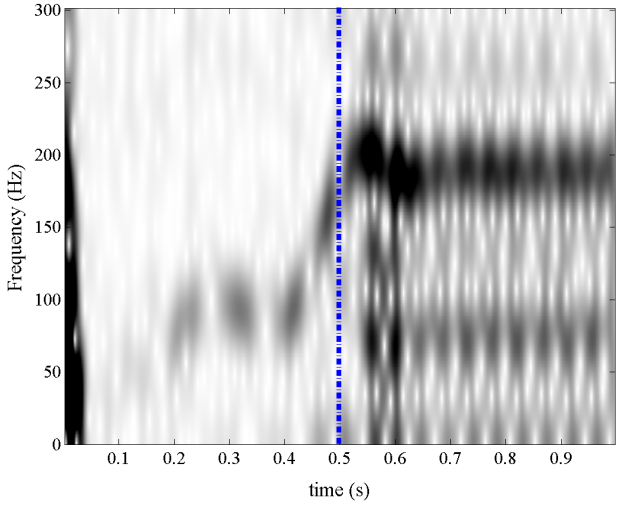

Fig.8. STFT spectrogram of the filtered current obtained using a Gaussian window with 50 points.

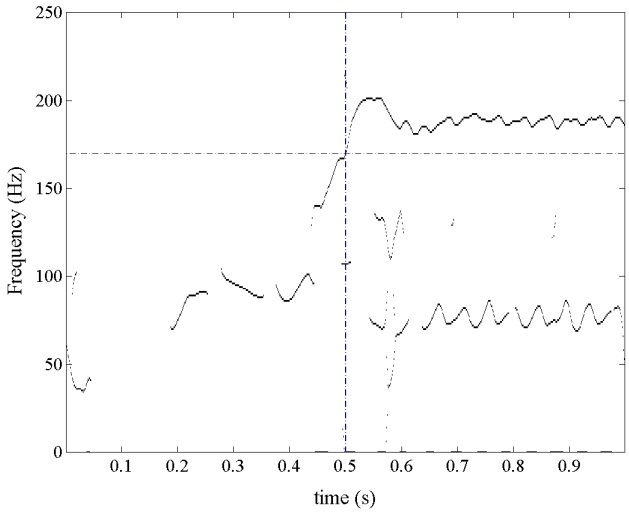

Fig.9. Ridges of the STFT spectrogram.

The corresponding spectrogram, $P_W f(u,\xi)$ shown in Fig. 11 is obtained by linearization of the logarithmic scalogram for the AWT, defined by (5) to (14). The scalogram, $P_W f(u,s)$, is obtained using six scales, selected as powers of two, $s^{-1} = \{2,4,8,16,32,64\}$. An interpolation with 12 voices is also performed. The modulating frequency, η, and the variance, σ, are chosen as 5.0 rad/s and 1.0 s respectively.

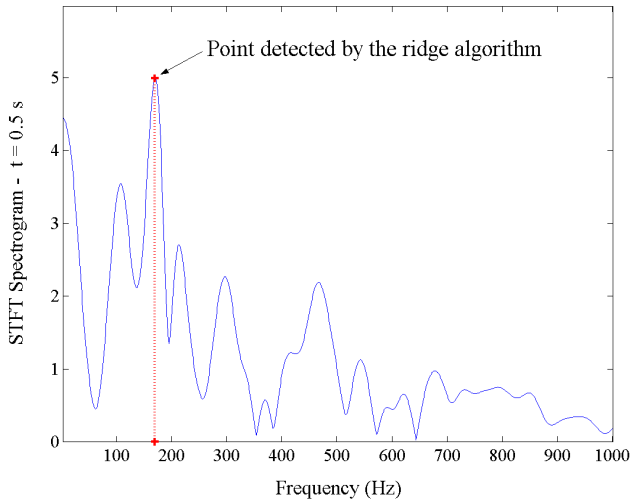

Fig.10. STFT spectrogram at the instant t = 0.5 s.

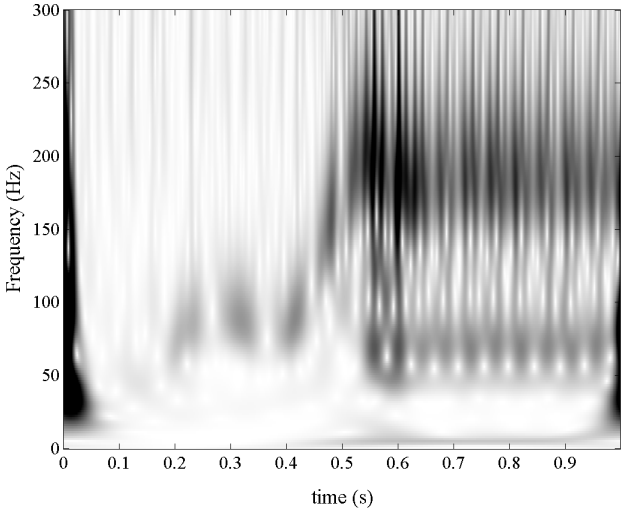

Fig.11. AWT spectrogram of the stator current

Fig. 12 shows the instantaneous frequencies after the use of the ridges algorithm. In this case less information is lost in the transients and that the resolution is better than that of Fig. 9. Fig. 13 shows the spectrogram at the instant t=0.5 s, and the detected ridge. It is interesting to note that the ridges in Fig. 12 of the AWT near this point (t=0.5 s) have an oscillation not detected by the opto-encoder (Fig.5, 10 ms between samples) or the STFT, probably because the resolution of the wavelet method is better than the others. In general the AWT algorithm can track fast fluctuations better and can be used for measuring the rotor speed of AC machines.

Faster ridge detection is obtained when the AWT spectrogram is used, because it is a smoother function than the STFT. Computation time required by AWT is approximately 40% lesser than STFT because the spectrogram is obtained with only 6 different scales and interpolation of 12 voices per scale (2048x72). The STFT requires 2048 FFT to perform a similar task (2048x2048). All estimations are obtained with off-line processing. A conventional FFT algorithm is used to calculate the AWT.

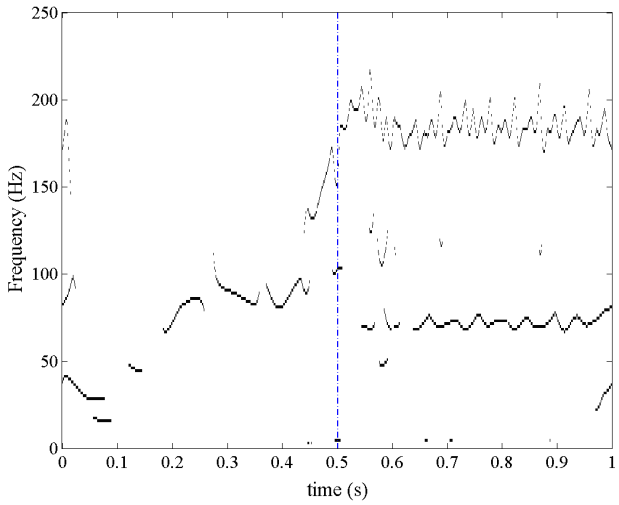

Fig.12. Ridges of the AWT spectrogram of the stator current

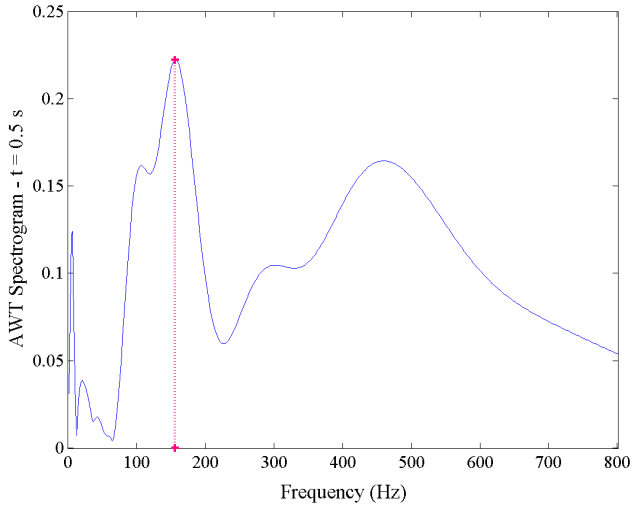

Fig.13. Detail of the AWT spectrogram for instant t = 0.5 s.

CONCLUSIONS

The AWT has been shown to be suitable for measuring the rotor speed of AC machines, during transient or steady-state condition, over the entire speed range. The method can be implemented in real time on a DSP. Compared to the STFT, a better resolution is obtained during transients in the speed with the AWT, even in the low speed range. The FFT algorithm can be adapted for wavelet transformation or a fast wavelet algorithm can be used to perform the real time calculations. The

method can be integrated into DTC drives that use wavelet torque filters with a little increase in computation time. The ridges algorithm is a simple and powerful way to improve the time-frequency resolution for sensorless speed estimation.

REFERENCES

[1] P. Vas, *Sensorless vector and direct torque control*, Oxford University Press, 1998.

[2] K.D. Hurst, and T.G. Habetler, "A comparison of spectrum estimation techniques for sensorless speed detection in induction machines," *IEEE Transactions on Industry Applications*, vol. 33, no.4, pp. 898-905, 1997.

[3] J. Restrepo and P. Bowler, "Analysis of induction machine slot harmonics in the tf domain," *IEEE Proceedings of the First International Caracas Conference on Devices, Circuits and Systems*, Caracas, Venezuela, pp. 127-130, 1995.

[4] J.A. Restrepo, M.I. Gimenez, V.M. Guzman, J.M. Aller, and A. Bueno, "Kernel selection for sensorless speed measurement of AC machines (Wigner vs. Page representation)," *IEEE Proceeding of Industry Electronics Conference IECON'98*, vol. 2, pp. 991-996, Aachen, Germany, 1998.

[5] S. Mallat, *A wavelet tour of signal processing*, Academic Press, 1999.

[6] N. Delprat, B. Escudié, P. Guillemain, R. Kroland-Martinet, P. Tchamitchian, and B. Torrésani, "Asymptotic wavelet and Gabor analysis: extraction of instantaneous frequencies," *IEEE Transactions on Information Theory*, vol. 38, no. 2, pp. 644-664, March 1992.

[7] M. Depenbrock, "Direct Self-Control (DSC) of Inverter-Fed Induction Machine," *IEEE Transactions on Power Electronics*, vol.3, no.4, pp.420-429, October 1988.

[8] T. Naguchi and I. Takahashi, "A new quick-response and high-efficiency control strategy of an induction motor," *IEEE Transactions on Industry Applications*, vol. 22, no. 5, pp. 820-827, 1986.

[9] J. Nash, "Direct torque control, induction motor vector control without an encoder," *IEEE Transactions on Industry Applications*, vol. 33, no. 2, pp. 333-341, 1997.

[10] J.A. Restrepo, J.M. Aller, T. Pagá, V.M. Guzmán, A. Buen and M.I. Giménez, "Direct torque control of the induction machine using field oriented method and time frequency transformation for speed estimation and parameter adaptation," *Proceedings of the International Conference on Electrical Machines ICEM'2000*, vol. 2, pp. 1105-1109, Helsinki, Finland, August 2000.

[11] N. Kasa, and H. Watanabe, "A torque ripples compensating technique based on disturbance observer with wavelet transform for sensorless induction motor drive," in *IEEE Proceedings of Industry Electronics Conference IECON'98*, vol. 2, pp. 580-585, Aachen, Germany, 1998.

0-7803-6618-8/01/$10.00 (C) 2001 IEEE